ORIGINAL PAPER

High-intensity monsoon rainfall variability and its attributes: a case study for Upper Ganges Catchment in the Indian Himalaya during 1901–2013

Alok Bhardwaj[1] · Robert J. Wasson[2,3] · Winston T. L. Chow[4] · Alan D. Ziegler[5]

Abstract

High-intensity monsoon rainfall in the Indian Himalaya generates multiple environmental hazards. This study examines the variability in long-term trends (1901–2013) in the intensity and frequency of high-intensity monsoon rainfall events of varying depths (high, very high and extreme) in the Upper Ganges Catchment in the Indian Himalaya. Using trend analysis on the Indian Meteorological Department (IMD) rainfall dataset, we find statistically significant positive trends in all categories of monsoon rainfall intensity and frequency over the 113-year period. The majority of the trends for both intensity and frequency are spatially located in the Higher Himalayan region encompassing upstream sections of the Mandakini, Alaknanda and Bhagirathi River systems. The extreme rainfall trends for both intensity and frequency are found to be only located in the vicinity of the upstream section of the Mandakini Catchment. Further, we explored the relationship between the Arctic Oscillation (AO) climate system and the frequency of occurrence of high-intensity rainfall events. Results indicate that AO is more likely to influence the occurrence of extreme monsoon events when it has a higher magnitude of negative AO phase. This study will help in better understanding of the influence of climate change at higher latitudes on mid-latitude rainfall extremes, particularly in the Himalayas. The implications of the findings are that statistically significant increasing rainfall depths and frequency in the Higher Himalayan region support the notion of higher frequency of rainfall-induced hazards in the future.

Keywords Ganges · Indian Himalaya · Extreme rainfall · Arctic Oscillation

✉ Alok Bhardwaj
  alok.bhardwaj@ce.iitr.ac.in

[1] Department of Civil Engineering, Indian Institute of Technology, Roorkee, India

[2] School of Science and Engineering, James Cook University, Cairns, QLD, Australia

[3] Fenner School of Environment and Society, Australian National University, ACT, Canberra, Australia

[4] School of Social Sciences, Singapore Management University, Singapore, Singapore

[5] Faculty of Fisheries and Aquatic Resources, Mae Joe University, Chiang Mai, Thailand

1 Introduction

1.1 Trends of high-intensity rainfall in the Himalayan Region

High-intensity monsoon rainfall events in the Indian Himalaya generate multiple hazards including large landslides, flash floods, landslide lake outburst floods (LLOFs), glacial lake outburst floods (GLOFs) and debris flows (Ives 2004; Bookhagen 2010; Ziegler et al. 2014, 2016). High-intensity monsoon rainfall and LLOFs are suggested to be the primary causes of large floods in the Upper Ganges Catchment over the last 1000 years (Wasson et al. 2013; Srivastava et al. 2017). In June 2013, high-intensity monsoon rainfall created a compound hazard consisting of a large flash flood, hundreds of shallow landslides, numerous LLOFs and a small GLOF in the Upper Ganges Catchment in the Indian Himalaya (Kala 2014; Sati and Gahalaut 2013; Dobhal et al. 2013; Ziegler et al. 2014). Some examples of rainfall induced large floods in the region include the 2014 flood in the Western Himalayas, the 2010 flood in the Indus River Basin and the 1970 flood in the Central Indian Himalayas (Hartmann and Buchanan 2014; Wasson et al. 2013).

It is, therefore, important to understand the characteristics of high-intensity rainfall events in the high mountainous areas of the Himalayas. In this study, we focus on the Upper Ganges Catchment, which is the one of the largest river catchments in the Himalayas and North India (Wester et al. 2019) (Fig. 1). Specifically, we focus on the detection of trends in high-intensity monsoon rainfall because (a) monsoon rainfall represent 85% of the total rainfall received in the region (Asthana and Sah 2007), and (b) during the monsoon season hundreds of tourists visit this region when the probability of occurrence of rain-induced hazards is high. Secondly, we investigate the climatological drivers of high-intensity rainfalls, first through a comprehensive review of the known climatological reasons and then
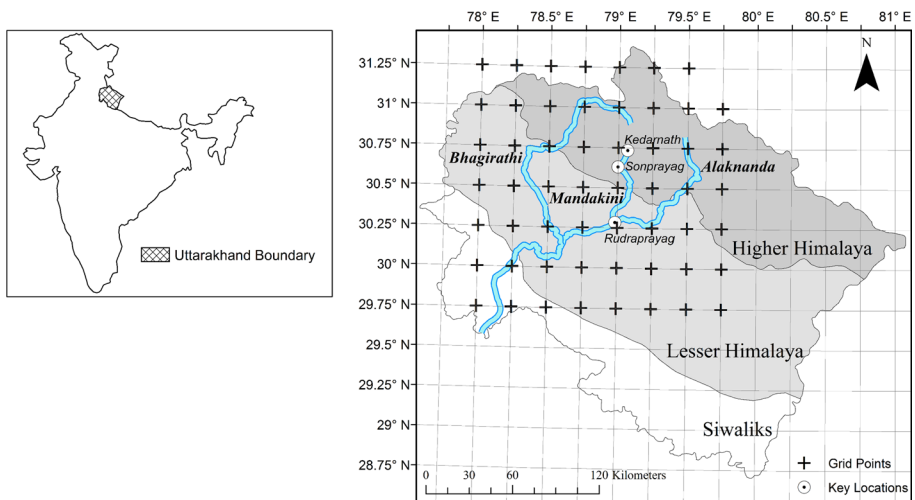
Fig. 1 Mandakini, Alaknanda and Bhagirathi Rivers form the Upper Ganges Catchment in Uttarakhand, North India. There are 55 IMD grid points in and surrounding the Upper Ganges Catchment (black cross). The grid spacing is 0.25° spanning latitudes of 29.75°N to 31.25°N and longitudes of 78.0°E to 79.75°E. Kedarnath, Sonprayag and Rudraprayag are located along the Mandakini River where huge damages were reported after the 2013 flood

exploring any potential influence of the synoptic climate system of the Arctic Oscillation that is not studied in detail previously for the Upper Ganges Catchment.

Trends of high-intensity rainfall events including extreme events have been investigated for the whole of India including certain parts of the Himalayas (May 2004; Roy and Balling 2004; Goswami 2006; Rajeevan et al. 2008; Roy 2009; Krishnamurthy et al. 2009; Ghosh et al. 2009; Naidu et al. 2009; Guhathakurta et al. 2011; Ghosh et al. 2012; Vittal et al. 2013). Overall summary of these studies includes (a) increased frequency of extreme rainfall events in central, northwest, eastern coastal regions and southern regions of India, (b) increasing frequency of extreme events at the rate of 6 to 10% per decade with major changes in the trends happening around 1975, (c) decreasing frequency of moderate events since 1980s and (d) some studies showing both increasing and decreasing trends in extreme rainfall events in Northeast India, Himalayan foothills and Indo-Gangetic plains. Fewer trend detection studies of high-intensity rainfalls exist for the Indian Himalayas (Joshi et al. 2006; Bhutiyani et al. 2009; Nandargi and Dhar 2011; Singh and Mal 2014; Mukherjee et al. 2015; Bharti et al. 2016; Zaz et al. 2019). Some of the major findings from these studies are: (a) when station rainfall data are used to detect trends: decreasing trend in total monsoon rainfall, increased frequency of extreme rainfall events during 1950s and early 1990s and decreased frequency of extreme rainfall events during late 1990s and 2000s; (b) when gridded rainfall products are used to detect trends: excessive monsoon rainfall in the central Himalayas from 1980 to 2000s, alternate scant and excessive monsoon rainfall periods in the western Himalayas, no significant overall trend in the frequency of extreme rainfall for the entire Himalayan region. In addition, trend studies have been conducted in the neighborhood of the Himalayas including the Indus Basin (Archer and Fowler 2004; Hartmann and Buchanan 2014), Hindu-Kush Himalayas (Zhan et al. 2017), Nepal Himalayas (Shrestha et al. 2017) and South Asia (Sheikh et al. 2015). These studies reveal increasing occurrences of extreme monsoon events in the Northern part of the Himalayas and the Tibetan Plateau, together with increased occurrences of wet days of 1-day, 3-day and 5-day durations in the Hindu-Kush Himalayas.

Overall, in the Himalayas, there is some evidence of higher occurrences of extreme rainfall events that are not spatially consistent, suggesting that different parts of the Himalayas are exposed differently to extreme events. For example, a sub-section of the Western Himalayas known as Uttarakhand, where the Upper Ganges Catchment is located, was found to be most exposed to extreme events (Bharti et al. 2016). Therefore, extreme rainfall trends should be studied at a local scale in the Himalayas to reveal specific trends, as rainfall characteristics could be different when studied at a local scale compared to a regional scale (Ghosh et al. 2009, 2012; Sheikh et al. 2015). Therefore, we have chosen to investigate the long-term trends in the intensity and frequency of high-intensity monsoon rainfall events for the Upper Ganges Catchment in Uttarakhand that includes Alaknanda, Mandakini and Bhagirathi River Basins (Fig. 1).

1.2 Climatological reasons causing high-intensity monsoon rainfall in the Himalayas

Major contributors to the monsoon rainfall in the Indian Himalayas include (a) regional drivers that include the Indian Monsoon system providing moisture from the Bay of Bengal and/or the Arabian Sea (Joseph et al. 2015), and the sub-tropical storms embedded in the Westerlies (Dimri and Chevuturi 2016), (b) global teleconnections comprising of (i) El Niño-Southern Oscillation (Kumar et al. 1999; Krishnamurthy and Goswami 2000; Yadav

et al. 2009), and its effect being modulated by the Indian Ocean Dipole (IOD) (Ashok et al. 2001, 2004; Behera et al. 2005), (ii) Arctic Multidecadal Oscillation (AMO) (Goswami et al. 2006), (iii) Pacific Decadal Oscillation (Krishnan and Sugi 2003; Krishnamurthy and Krishnamurthy 2014) and (iv) Arctic Oscillation (AO) modulated by the Arctic Amplification (AA) (Coumou et al. 2018). The effect of the AO and its possible modulation by the AA on the occurrence of midlatitude extremes is an active area of research in the climate research community (Cohen et al. 2020). We first review the interaction of regional drivers, followed by a review of global teleconnections that are affecting the rainfall occurrences in the Indian Himalaya.

1.2.1 Regional drivers

The low-level monsoon flow from the Arabian Sea/Bay of Bengal transports the moisture that is orographically lifted in the Himalayas (Joseph et al. 2015). The upper-level sub-tropical storms that are generated in the Mediterranean region are embedded in the West-erlies and flow toward the Himalayas. A deep enclosure is created leading to the incursion of upper-level sub-tropical storms toward the Himalayas that interacts with the lower-level moisture flow. It has been found that the bifurcation of the Tibetan High (TH) helps in the setup of this deep enclosure connecting lower to upper levels (Vellore et al. 2016) and leads to a strong convection that causes heavy rainfall in the Himalayas (Houze Jr. et al. 2017). Recently, Vellore et al. (2019) suggested that potential vorticity from upper levels and higher latitudes are channelized horizontally as well as vertically to lower levels, thus increasing the chances of heavier rainfall in the Himalayas.

1.2.2 Global teleconnections

In recent decades, the influence of the ENSO on the Indian monsoon rainfall is found to be weakening (Kumar et al. 1999), i.e., during warm phases of ENSO (El Niño), a weak monsoon is not observed as expected, and during cold phases of ENSO (La Niña), strong monsoons do not prevail as expected. However, this only happens if the interannual and the interdecadal phases are different (Krishnamurthy and Goswami 2000). Further, the ENSO–Indian monsoon relationship is found to be modulated by the existence of the Indian Ocean sea surface temperature (SST) anomalies represented by the IOD (Ashok et al. 2001). The ENSO effect is reduced if the ENSO and IOD phases are same, indicating that the IOD is also an independent driver of the monsoon rainfall (Ashok et al. 2004; Behera et al. 2005; Wang et al. 2016). It was reported that the IOD affects the monsoon rainfall through the generation of a regional Hadley circulation, while the changes in the planetary Walker circulation have led to the reduced effect of the ENSO (Pokhrel et al. 2012). Within this context, Kumar et al. (1999) indicated that the role of the land-sea heat contrast is more prominent in driving the monsoon rainfall due to the recent trend in mid-latitude warming. According to Pokhrel et al. (2012), the land-sea heat contrast is important to drive only the early monsoon rainfall, while it is the tropospheric temperature (TT) gradient that maintains the intensity of the flow throughout the monsoon season. Strong TT anomalies can be generated by north Atlantic SST anomalies represented by the AMO through the strong positive North Atlantic Oscillation (NAO) that maintains the intensity of the monsoon rainfall throughout the season (Goswami et al. 2006; Kucharski et al. 2009). Yadav et al. (2020) described that south Atlantic SST dipoles intensify ITCZ that

generates a stationary wave resembling circum-global teleconnection pattern that can cause higher amounts of monsoon rainfall in north central India.

Further, the PDO, which represents decadal phenomena in the Pacific Ocean, also influences the Indian monsoon (Krishnan and Sugi 2003). The Pacific SST variations linked with the PDO have an inverse relationship with the Indian monsoon rainfall, such that warm phases of the PDO are associated with decrease in the monsoon rainfall and vice-versa (Krishnan and Sugi 2003; Krishnamurthy and Krishnamurthy 2014). Roy et al. (2003) found the inverse relationship with the monsoon rainfall in the central and southern India. Dry monsoon seasons or drought-like conditions occur during simultaneous occurrences of the warm phase of the PDO and the El-Niño, and wet monsoon seasons occur during simultaneous occurrences of the cold phase of the PDO and the La-Niña (Krishnan and Sugi 2003). Krishnamurthy and Krishnamurthy (2014) proposed that changes in the equatorial Hadley circulation system caused by changes in the trade winds affect the monsoon rainfall.

Presently, the climate research is focused on developing an understanding of the influence of the Arctic warming in causing mid-latitude extremes including extreme rainfalls in the Himalayas. The warming of the Arctic region is known as Arctic Amplification (AA), which is twice as fast as the mid-latitudes (Cohen et al. 2014). Such warming causes weakening of the polar vortex that further causes changes in the movement of planetary Rossby waves (Cohen et al. 2014, 2020). Under such conditions, Rossby waves could become more stagnant and amplified leading to blocking and affects the mid-latitude weather. Many researchers are attributing the occurrence of mid-latitude extremes to AA through Rossby waves (Boers et al. 2019). Such climatic conditions can be captured by the hemispherical wide synoptic system of the Arctic Oscillation (AO) (Coumou et al. 2018) because the negative phase of the AO resembles the weakening of the Rossby waves. Further, AO can influence the amount of snow-cover in Eurasia that directly affects the land-sea thermal gradient that plays a role in modulating the strength of the Indian monsoon (Kumar et al. 1999; Yeo et al. 2017). Rajeevan (2018) suggested that AO can influence monsoon rainfall in north India and latent heat released by higher rainfall depths is transported towards the Arctic region through planetary waves causing Arctic sea ice loss. This indicates a two-way feedback loop between the Arctic climate and heavy Himalayan rainfall.

Some studies have found linkages between AO/NAO and rainfall occurrences in the Himalayas. Yadav (2010) found statistically significant correlation between reconstructed tree-ring-based premonsoon precipitation and positive NAO from 1825–1999, due to strengthened westerlies, and positive correlation with NINO3-SST index except from 1930–1960, due to warm phases of the AMO. Roy (2011) examined the role of monthly NAO in influencing peak monsoon rainfall across India except Uttarakhand and northern states from 1871–2002 and found stronger positive correlation between peak monsoon rainfall amounts and August and September NAO, while stronger negative correlation with February NAO. Joseph et al. (2015) indicated that cold air from the Arctic region intruded into the mid-latitudes during negative AO phase and interacted with the upper tropospheric westerly trough to trigger extreme rainfall for two days leading to the flash flood in 2013. Sharma et al. (2017) analyzed the relationship between occurrences of palaeo-floods and a proxy of AO and found that negative phases of AO were associated with four major palaeo-flood clusters that occurred in the middle Satluj valley in the western Himalayas. Agnihotri et al. (2017) concluded that negative AO anomalies during March lead to positive summer monsoon rainfall anomalies over the UKS region (Kashmir, Himachal Pradesh and Uttarakhand), and positive Eurasian snow cover extent (SCE) during March leads to above normal monsoon rainfall over the

UKS region. Xavier et al. (2018) examined the role of NAO in causing high precipitation in June 2013 that led to the massive flood in north India and found decreased intensity of westerlies had caused cold Arctic air to move southwards that was associated with daily negative NAO during the event. However, monthly NAO for June 2013 was found to be positive.

Apart from monsoon rainfall, some authors have also examined the effect of AO on winter rainfall. Roy (2011) found stronger negative correlation between NAO index and winter rainfall across the Indian sub-continent ranging from arid regions in northwest to wetter regions in northeast India from 1871–2002. Kar and Rana (2014) found higher magnitudes of winter precipitation anomaly in northwest India and surrounding region is associated with the second principal component of interannual 200 hPa zonal winds in northern hemisphere, which has a positive correlation with AO/NAO during 1979/1980–2009/2010. This indicates that with higher magnitudes of AO/NAO larger magnitudes of winter precipitation are expected in northwest India and surrounding region. Midhuna and Dimri (2018) found positive AO phases associated with higher winter precipitation over the western Himalayas during 1979–2018; strong westerlies, strong north–south temperature gradient supporting upward flow and weaker Hadley cell conditions were present during positive AO years that increased the strength of western disturbances causing higher winter rainfall. Yadav (2020) found that AO/NAO had statistically significant relationship with winter rainfall over northwest India prior to 1979, while ENSO had statistically significant relationship after 1979.

With this motivation, we are exploring the effect of the AO on high-intensity monsoon rainfall in the Upper Ganges Catchment in the Indian Himalayas, in an effort to contribute to and constrain the ongoing debate of the influence of climate change in higher latitudes to occurrences of extremes in the mid-latitudes. From the outset, we wish to make it clear that we are not focusing on exploring any mechanisms through which AO will cause high-intensity monsoon rainfall events. Our aim with this research is to ascertain if there is any linkage between the synoptic climate forcing system of the AO and high-intensity monsoon rainfall in the Indian Himalayas.

2 Study area

The Upper Ganges Catchment in the Indian Himalaya (also known as the Garhwal Himalaya) is located at the western end of the Central Himalaya in the Uttarakhand State of India and comprises of Alaknanda, Mandakini and Bhagirathi catchments (Fig. 1). The study area spans latitudes from 29.75°N to 31.25°N and longitudes from 78°E to 79.75°E. The three rivers cross the Main Central Thrust (MCT) that separates the Higher Himalaya from the Lesser Himalaya (Fig. 1). The MCT zone is composed of many faults, fractured and weathered rocks, zones of high relief and steep gradient streams with steep hill slopes along the stream edges (Asthana and Sah 2007; Wasson et al. 2008). This geologically geomorphologically sensitive environment is susceptible to slope failures in response to various triggers, including earthquakes and high-intensity rainfall events. During the monsoon season, the area is primed for rainfall-induced hazards including large landslides, debris flows, GLOFs and LLOFs, as witnessed in June 2013 when over a 2-day period an estimated 300 mm of rainfall fell in some locations (Kala 2014; Sati and Gahalaut 2013; Dobhal et al. 2013).

3 Data and methods

3.1 Rainfall data

To analyze high-intensity rainfalls, we have selected the 0.25° gridded daily rainfall dataset from the Indian Meteorological Department (IMD) available from 1901 to 2013. The rationale to select the IMD dataset is based on our previous study (Bhardwaj et al. 2017), which compared four rainfall datasets including IMD, TRMM, APHRODITE and PERSIANN against ground stations using statistical indices such as mean bias error, root mean square error, probability of detection, false alarm ratio, false positive rate and receiver operating curves. We also found that the IMD product performed better than others in replicating the high-intensity rainfall depths during the 2013 flash flood event in Uttarakhand (Bhardwaj et al. 2017). The IMD product is capable of estimating rainfall that may have been influenced by the topography of a region. For example, Pai et al. (2014) described that the IMD product captured the rainfall distribution across the high terrain of the Western Ghats in the west of India. Likewise, Bhardwaj et al. (2017) found that the IMD product was able to estimate depths at ground stations located at different terrain heights across the Garhwal Himalaya. Further, it is the only product with daily rainfall data for the twentieth century in the Indian Himalaya. The IMD gridded dataset is developed for India using a total of 6955 rainfall stations from 1901 to 2013 at a spatial resolution of 0.25° (Pai et al. 2014). According to Pai et al. (2014), a quality control check is performed on the raw rainfall data to remove spurious values. The data are then inputted to a 0.25° grid using an inverse distance weighted interpolation scheme to create the final IMD gridded product. The inverse distance weighting interpolation scheme is based on the methodology from Shepard (1968) that defines a radius of influence and all the stations within the radius are considered for interpolation. We obtained the product from the IMD website (www.imdpune.gov.in). For more information on the methods used to develop the product, see Pai et al. (2014).

3.2 Definition of high-intensity rainfall depths

At each of the 55 IMD grid points spanning the Upper Ganges Catchment, we constructed a series of daily monsoon rainfall data from June to September extracted from each year from 1901 to 2013. At each grid point, we considered three sub-categories of high-intensity rainfall depths namely high, very high and extreme when rainfall depths exceed 90th, 95th and 99th percentile thresholds of the constructed monsoon rainfall time series from 1901–2013 (including wet and dry days), respectively (Ghosh et al. 2009; Bharti et al. 2016; Vittal et al. 2013).

At each grid point, we consider two key properties of rainfall events, frequency and intensity. Frequency is the total number of rainfall events exceeding a certain threshold value (high, very high, and extreme) occurring in a single year in the monsoon season, whereas intensity is the sum of those rainfall depths. For example, the grid point at (78.00°, 30.00°) had three extreme rainfall events in 2013: June 16 (109.6 mm), June 17 (219.6 mm) and Aug 6 (110.2 mm) exceeding the 99th threshold value of 96.64 mm at this grid point. Thus, the extreme intensity at this grid point is 439.4 mm, and the extreme frequency is 3 for the year 2013.

3.3 Trend detection methods

We used the nonparametric Mann–Kendall test (Kendall 1975; Mann 1945) and the Sen Slope (Sen 1968) estimator to detect the statistical significance and magnitude of trends in intensity and frequency of rainfall events in the 1901–2013 rainfall time series at each grid point (see supplementary for the description of the methods). Nonparametric tests were used because these tests do not assume any prior statistical distribution of data.

Prior to trend detection analysis, we reduced serial correlation among data points using pre-whitening (PW) and variance correction (VC) methods (Salas et al. 1980; Kulkarni and von Storch 1995; Hamed and Rao 1998; Yue and Wang 2004) (see supplementary section for the description of the methods). The PW approach considers the correlation at a lag-1 for the entire series, whereas the VC approach takes into account the complete correlation structure of the series and better represents the process of the removal of serial correlation from the time series.

3.4 Arctic Oscillation (AO) index data

The AO is defined as the empirical orthogonal function (EOF) of the anomalies in the monthly sea level pressure at 1000-hpa (pressure level) over the region poleward of 20^0 N (Thompson and Wallace 1998). The associated principal component series is the AO index. The AO is operationally quantified by the AO index, which fluctuates between positive and negative phases. During a positive phase, surface pressure in the Arctic region is low that strengthens the mid-latitude jet stream that restricts the cold Arctic air within the Arctic region, while the polar winds flow toward the mid-latitudes due to high pressure in the Arctic region during a negative phase. For our analysis, we downloaded monthly AO index time series from 1900 to 2013 from NOAA monthly AO webpage (www.esrl.noaa.gov/psd/data/20thC_Rean/timeseries/monthly/AO/).

4 Results and discussion

4.1 Trends in intensity and frequency of high-intensity monsoon rainfall events

We found statistically significant increasing trends in rainfall intensity across all the three thresholds for both the PW and VC methods (Fig. 2; magnitude of trends for 90th, 95th and 99th percentile thresholds is shown in Tables S1, S3 and S5 of supplementary, respectively). Slope magnitudes of statistically significant trends in intensity are in the range of 1.07 to 3.00 mm/year, 0.58 to 2.15 mm/year and 0.28 to 1.18 mm/year for rainfall depths exceeding the 90th, 95th and 99th percentile thresholds, respectively (considering both the methods). In summary, trends in intensity are highest for the 90th percentile followed by the 95th and 99th percentile thresholds. This may be attributed to the lesser amount of available data as percentiles become higher. Further, the majority of the trends are spatially located in the Higher Himalayan region upstream of and in the vicinity of the Main Central Thrust (separating Higher from Lesser Himalaya), where major tourist places are located (Fig. 1).

Importantly, across all the thresholds, some statistically significant trends in rainfall intensity are obtained at grid points that are spatially close to tourist places, particularly
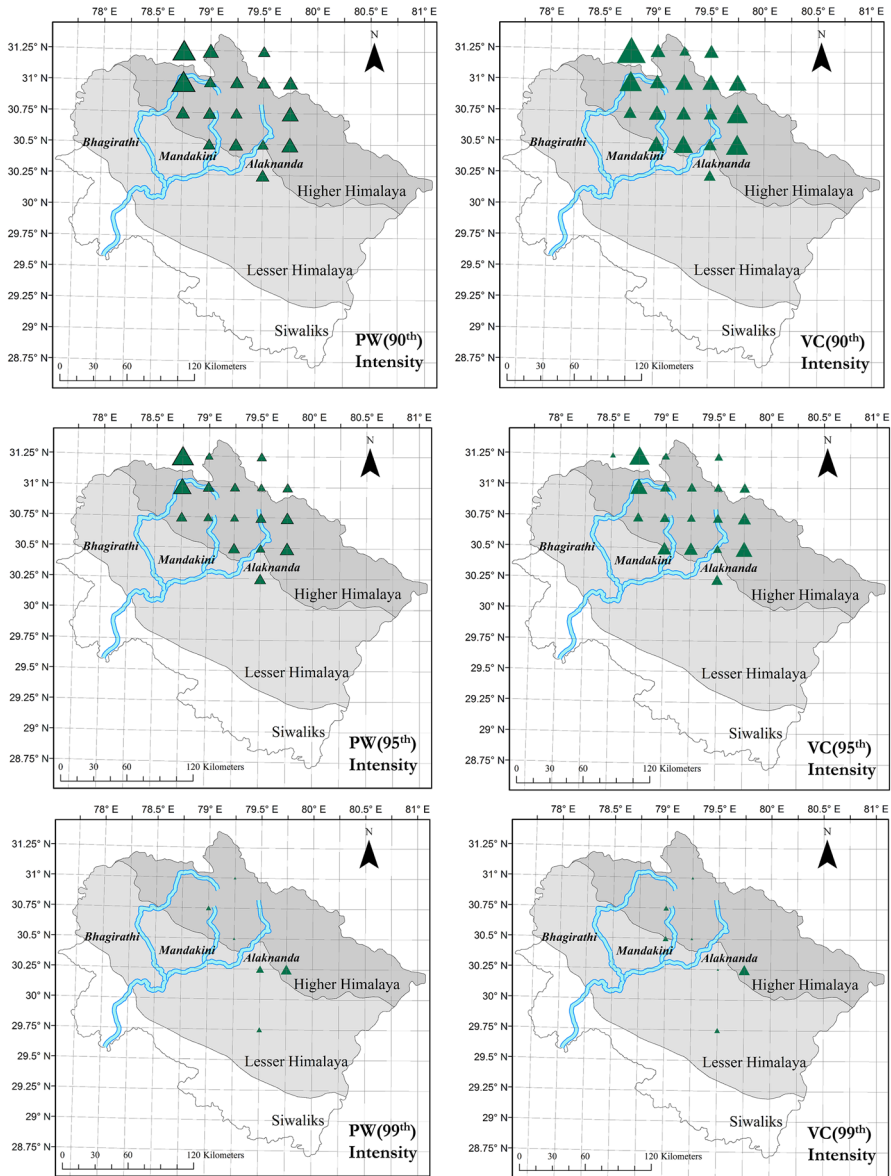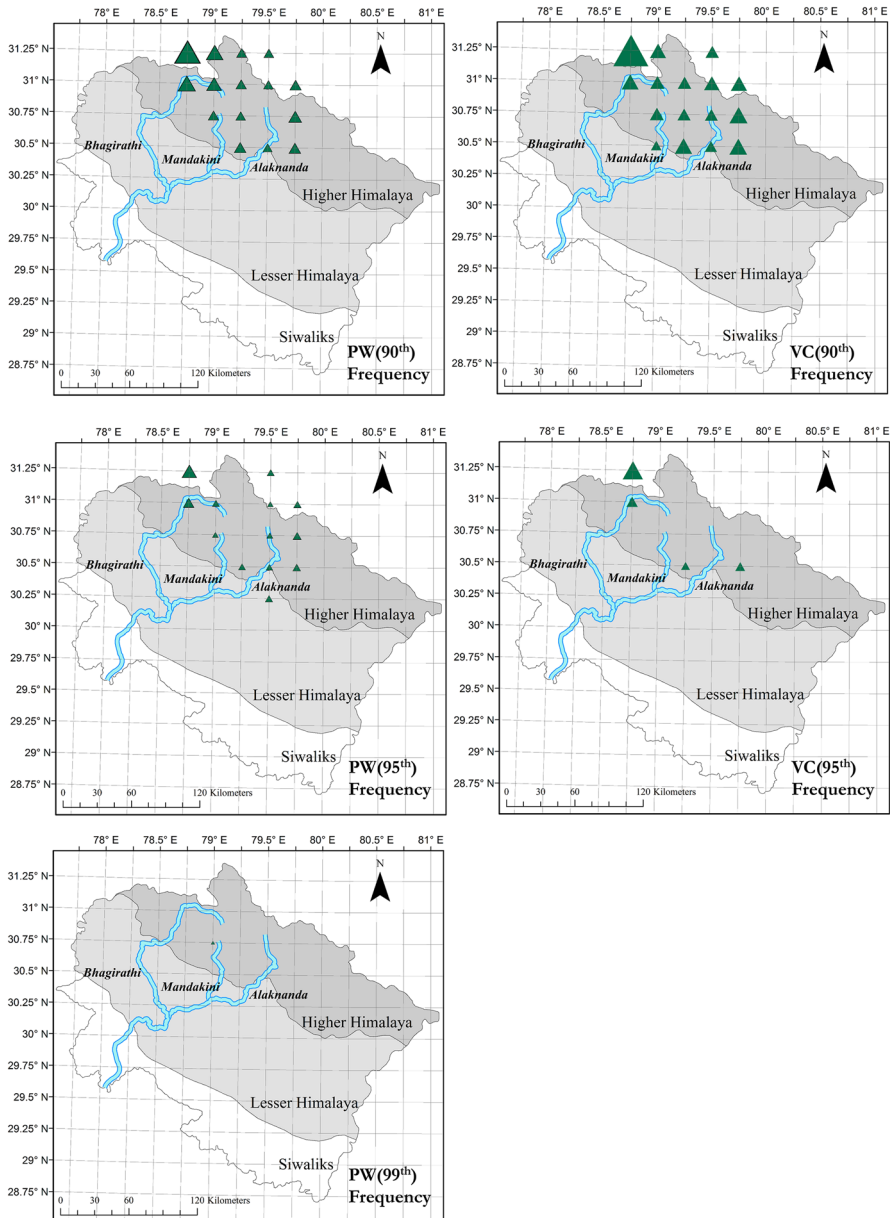
Fig. 2 Trends in rainfall intensity for depths exceeding 90th, 95th and 99th percentile thresholds. The trends are calculated using the PW (prewhitening) and VC (variance-correction) methods. Relative sizes of triangles represent relative slope magnitudes of statistically significant trends (Tables S1, S3, S5 of Supplementary shows magnitude of trends in rainfall intensity for 90th, 95th and 99th percentile thresholds, respectively)

for Kedarnath. The slope magnitudes at the grid point closest to the Kedarnath (79.00°, 30.75°) are 1.26 mm/year, 0.92 mm/year and 0.55 mm/year for 90th, 95th and 99th percentiles for the PW method, and 1.70 mm/year, 1.07 mm/year and 0.55 mm/year for 90th, 95th and 99th percentiles, respectively, considering the VC method.

We have also calculated statistically significant trends in rainfall frequency for the three thresholds (Fig. 3; magnitude of trends for 90th, 95th and 99th percentiles is shown


Fig. 3 Trends in rainfall frequency for depths exceeding 90th, 95th and 99th percentile thresholds. The trends are calculated using the PW (prewhitening) and VC (variance-correction) methods. Statistically significant trends were not obtained for the 99th percentile by the VC method and hence not shown. Relative sizes of triangles represent relative slope magnitudes of statistically significant trends (Tables S2, S4, S6 of Supplementary show magnitude of trends in rainfall frequency for 90th, 95th and 99th percentile thresholds, respectively)

in Tables S2, S4 and S6 of supplementary, respectively). Similar to the intensity trends, majority of the frequency trends were spatially located north as well as in the vicinity of the MCT in the Higher Himalayan region. A greater number of trends with higher magnitudes were obtained for rainfall events exceeding the 90th percentile threshold, followed by the 95th and 99th percentiles for both the methods. For the 99th percentile, only one statistically significant and increasing trend with a slope magnitude of 0.02 events/year is obtained in the close vicinity of Kedarnath by the PW method (Fig. 3; Table S6).

Collectively, majority of the statistically significant trends for both intensity and frequency of rainfall events exceeding the three thresholds are spatially located north of as well as in the vicinity of the MCT in the Higher Himalayan region. This section of the Indian Himalaya is fragile with unstable steep slopes that may lead to debris flows and landslides during high-intensity rainfall events and our results of increasing trends in both intensity and frequency hint to the possibility of a greater number of slope failures in future. All the trends, except for the 99th percentile trends, encompass upstream sections of Bhagirathi, Mandakini and Alaknanda River systems. The 99th percentile trends for both intensity and frequency are found to be located in the vicinity of the upstream section of the Mandakini Catchment. This implies that extreme rainfall depths will most likely affect the Mandakini Catchment, whereas comparatively smaller rainfall depths will affect all the river systems. As upstream sections of river systems have steep slopes, together with deep and narrow valleys, the danger of LLOFs may increase in future. The implications of these findings are that most of the grid points in the Higher Himalayan region now experience slightly more high-intensity rainfall events, which are of greater rainfall depths, than a century ago.

4.2 Relationship between elevation and location of intensity and frequency trends

Elevations were derived from a digital elevation model (DEM) with a spatial resolution of 30 m developed using CARTOSAT-1 satellite data (available at BHUVAN [Indian Geoplatform by ISRO]). Elevations in the Upper Ganges Catchment range from approximately 150 to 6000 m. Due to a large change in elevations, it is important to analyze the location of trends with respect to elevation changes across the study area. In Fig. 4, we show variation in statistically significant trends for rainfall intensity for depths exceeding 90th, 95th and 99th percentiles calculated using the PW and VC methods, with elevation. For the 90th and 95th percentile trends calculated using the PW and VC methods (Fig. 4 90_PW, 90_VC, 95_PW, 95_VC), we found trends with similar magnitude from 2000 to 2500 m; followed by an elevation gap of 500 m with no trends; next from 3000 to 4500 m, we found majority of the trends between 1 to 2 mm/year and few higher magnitude trends exceeding 2 mm/year for depths exceeding the 90th percentile; again we found an elevation gap from 4500–5000 m with very few trends at elevations nearer to 5000 m; finally, from 5000 to 5700 m, we observed majority of the 90th percentile trends had magnitudes between 1–2 mm/year, while majority of the 95th percentile trends were less than or equal to 1 mm/year. For the 99th percentile, majority of the trends had magnitudes smaller than 1 mm/year and were restricted only to a few elevation ranges including near to 1500 m, 2000–2500 m and 4500–5500 m. Overall, we found that majority of the 90th percentile trends are similar in magnitude across all the elevations; 95th percentile trends are similar in magnitude till 4500 m, beyond which trends are found to be smaller in magnitude; for the 99th percentile, smaller magnitude of trends was found between 2000–2500 m and approximately 5500 m. Collectively, for intensity trends we found no relationship between magnitude of trends and increase in elevations.
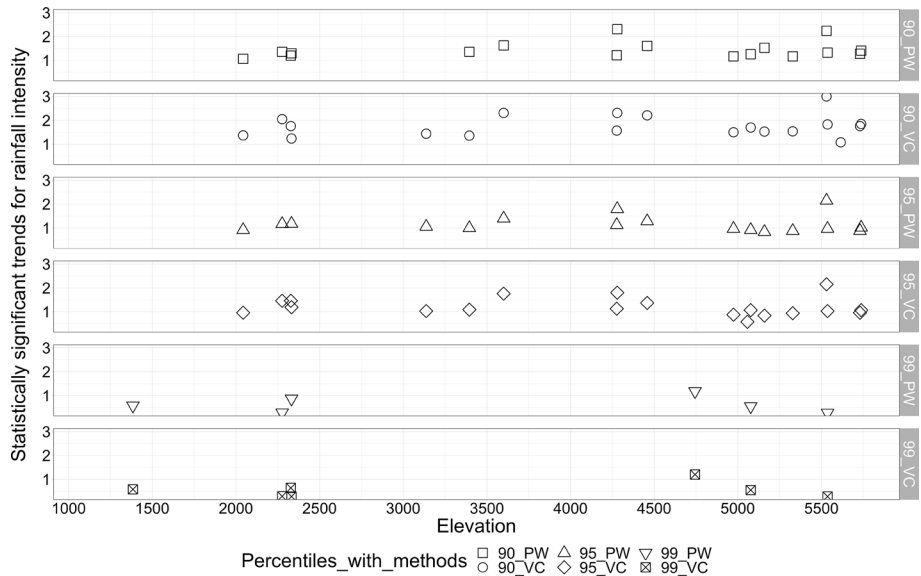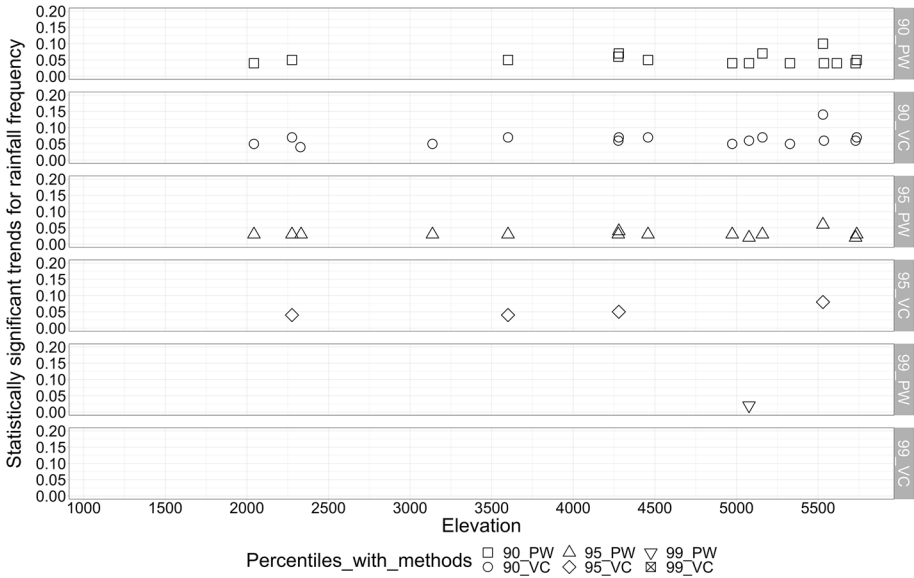
Fig. 4 Variation in statistically significant trends for rainfall intensity with respect to elevation in the Upper Ganges Catchment. Different symbols represent different methods used to calculate trends for depths exceeding a percentile threshold. For example, *90_PW* represents trends calculated for depths exceeding the 90th percentile using the PW method. Unit of trend is mm/year and unit of elevation is meter

Next, we studied the variation in statistically significant frequency trends with elevation (Fig. 5). For the 90th percentile, we found majority of the trends were approximately 0.05 events/year from 2000–5700 m (Fig. 5 90_PW, 90_VC). For the 95th percentile, most of the trends calculated using the PW method were less than 0.05 events/year from 2000–5700 m (Fig. 5 95_PW), while we obtained fewer trends with the VC method, but the magnitude of those trends increased with elevation (Fig. 5 95_VC). Finally, for the 99th percentile, we found a single trend at approximately 5000 m with the magnitude of 0.02 events/year calculated using the PW method. Overall, we found no general relationship between the magnitude of frequency trends and elevation. Collectively, we observed no relationship between the magnitude of intensity and frequency trends with elevation increase in the study area. This indicates that long-term trends are not dependent on the topography in the Upper Ganges Catchment.

### 4.3 Relationship between land use land cover and location of intensity and frequency trends

We examined the distribution of statistically significant trends in intensity and frequency across a land use land cover (LULC) distribution in the Upper Ganges Catchment. LULC classes were obtained from BHUVAN for 2011–2012 at a scale of 1:50,000 and can be accessed from https://bhuvan-app1.nrsc.gov.in/state/UK. Overall, we found only four LULC classes at the locations of statistically significant trends for intensity and frequency for all the thresholds including snow and glaciers, barren unculturable wasteland (or scrub land), evergreen forests (or semi evergreen forests) and grasslands (or grazing grounds) (Figs. 6, 7).

Fig. 5 Variation in statistically significant trends for rainfall frequency with respect to elevation in the Upper Ganges Catchment. Different symbols represent different methods used to calculate trends for depths exceeding a percentile threshold. For example, *90_PW* represents trends calculated for depths exceeding the 90th percentile using the PW method. Unit of trend is number of events/year and unit of elevation is meter
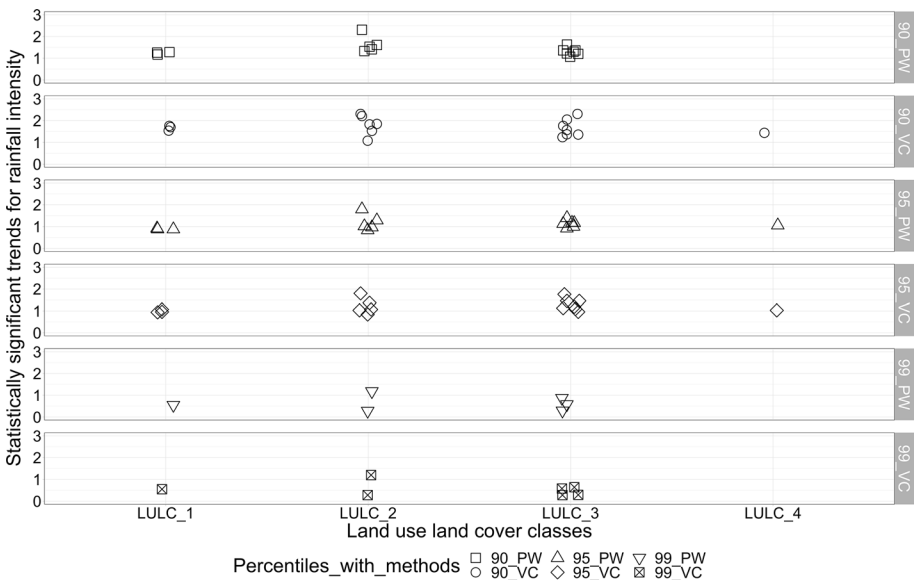
Fig. 6 Variation in statistically significant trends for rainfall intensity with respect to land use land cover (LULC) in the Upper Ganges Catchment. LULC_1: Snow and Glaciers; LULC_2: Barren unculturable wasteland/Scrub land; LULC_3: Evergreen forests/Semi-evergreen forests; LULC_4: Grasslands/grazing grounds. Different symbols represent different methods used to calculate trends for depths exceeding a percentile threshold. For example, *90_PW* represents trends calculated for depths exceeding the 90th percentile using the PW method. Unit of trend is mm/year. Data points are displaced horizontally by a small amount to show overlapping data points
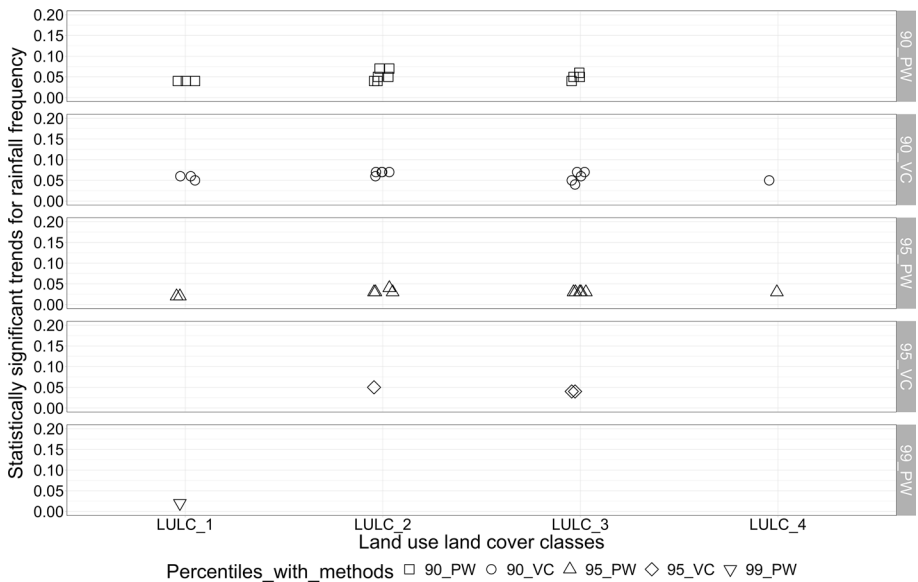
Fig. 7 Variation in statistically significant trends for rainfall frequency with respect to land use land cover (LULC) in the Upper Ganges Catchment. LULC_1: Snow and Glaciers; LULC_2: Barren unculturable wasteland/Scrub land; LULC_3: Evergreen forests/Semi-evergreen forests; LULC_4: Grasslands/grazing grounds. Different symbols represent different methods used to calculate trends for depths exceeding a percentile threshold. For example, *90_PW* represents trends calculated for depths exceeding the 90th percentile using the PW method. No trend was obtained for 99_VC. Unit of trend is number of events/year. Data points are displaced horizontally by a small amount to show overlapping data points

For rainfall intensity trends, we found the highest density of trends located in evergreen forests and the least number of trends located in grasslands (Fig. 6). Among the trends located in evergreen forests, we observed higher magnitude for the 90th percentile with the variance correction (VC) method and smaller magnitudes with less than 1 mm/year for the 99th percentile. Further, we found the second highest density of trends located in barren unculturable wasteland (or scrub lands), again with higher magnitudes of trends for the 90th percentile and smaller magnitudes for the 99th percentile. In areas of snow and glacier, we found fewer trends with magnitudes between 1–2 mm/year for the 90th and 95th percentiles, and less than 1 mm/year for the 99th percentile.

For rainfall frequency trends, we found the least density of trends located in grasslands with only a single trend for the 90th and 95th percentile each, and no trend for the 99th percentile (Fig. 7). Next, we obtained the second least density of trends located in snow and glaciers with higher magnitudes for the 90th percentile. Further, we found equivalent number of trends located in barren unculturable wasteland (or scrub lands) and evergreen forests, with equivalent magnitudes for the 90th and 95th percentile. We found only a single trend for the 99th percentile that was located in snow and glaciers.

Collectively, for trends in intensity and frequency, we found the least number of trends were located in grasslands, followed by snow and glacier areas. Higher density of trends was located in barren unculturable wasteland (or scrub lands) and evergreen forests. We found no trends located in agricultural lands or urbanized areas because these LULC classes are approximately located between 800–2000 m (Mishra and Chaudhuri 2015) where trends were not observed.

4.4 Relationship between large-scale rainfall events and AO in the Upper Ganges Catchment

We are interested in large-scale rainfall events in the Upper Ganges Catchment that are influenced by the AO synoptic climate system, which may play a role of translating these events in to wide-spread events that affect large areas of the catchment. For each of the sub-category (high, very high and extreme), we define large-scale events when rainfall depths exceed their respective percentile threshold values at least 75% (42 of 55 of the grid points) of the study area. The properties of such large-scale events are first explored, followed by an analysis to determine the influence of AO on such large-scale events in the next section.

4.4.1 Occurrence of large-scale monsoon rainfall events in the Upper Ganges Catchment

For the 90th percentile, 71 of 113 years had a total of 157 large-scale high-rainfall events in the Upper Ganges Catchment, with the highest frequency occurring in 2010 with 9 events and second highest frequency of 6 events each in 1901 and 1914 (Fig. 8a). At the decadal resolution (frequencies of large-scale events are added within each decade), higher frequency is observed during three decades from 1901 to 1930 with 29 events, 17 events and 22 events, respectively (Fig. 8b). After 1930, we observed a drop in the decadal frequency until 2000, followed by a higher decadal frequency from 2001–2010 with 15 events. For the decade from 2011–2020, we only had 3 years of data from 2011 to 2013 with a total of 10 events (Fig. 8b).
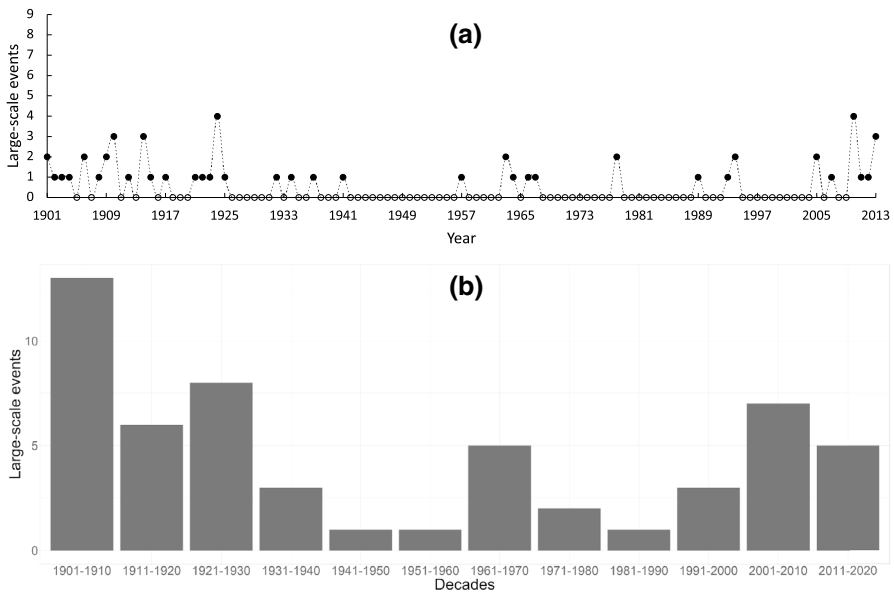
For the 95th percentile, 55 large-scale events were observed for 36 years with the highest frequency of 4 events in 2010 and 1924 and second highest frequency of 3 events in 2013, 1914 and 1910 (Fig. 9a). At the decadal resolution, we observed the highest frequency during 1901–1910 with 13 events, followed by a drop in the frequency with 6 and 8 events during 1911–1920 and 1921–1930, respectively (Fig. 9b). After 1930, decadal frequencies were lower with a slight increase observed during 1961–1970 with 5 events, until 2000. During 2001–2010 and 2011–2013, we observed 7 events and 5 events, respectively. It should be noted that 5 events occurred in three years (2011–2013) as compared to 7 events in the previous decade.

For the 99th percentile, we observed only 7 large-scale extreme events during 5 of 113 years, with the highest frequency of two events each in 1924 and 2013 (Fig. 10a). At the decadal resolution, the highest frequency of 3 events had occurred from 2011–2013 (Fig. 10b) indicating an increase in extreme events in the present times as compared to the previous years.

In summary, we found higher frequency of large-scale events during 1901–1930 and 2001–2013 for the 90th and 95th percentiles, while higher frequency for the 99th large-scale events was present in 1921–1930 and 2011–2013. Agnihotri et al. (2017) reported increased amounts of total monsoon rainfall during 1904–1924 and 2000–2013 using monthly rainfall amounts from the Global Precipitation Climatology Project (GPCP); the findings are consistent with our results of a higher frequency of monsoon events during the same periods. Additionally, frequency of large-scale events based on their occurrence in specific monsoon months is shown in Table 1. Frequency of events was higher for the month of July and August with 51 and 52 events for the 90th percentile, while September had the highest frequency for the 95th and 99th percentiles with 21 and 4 events,
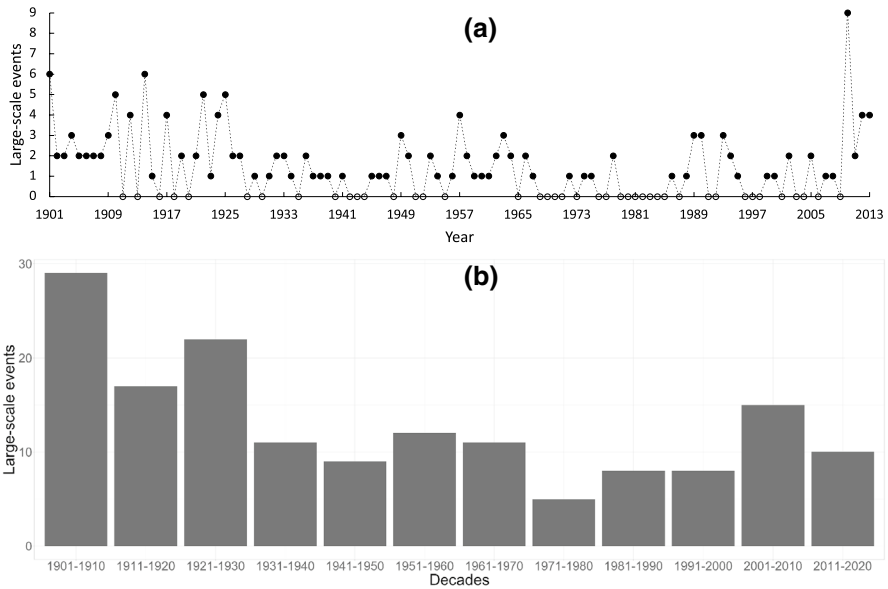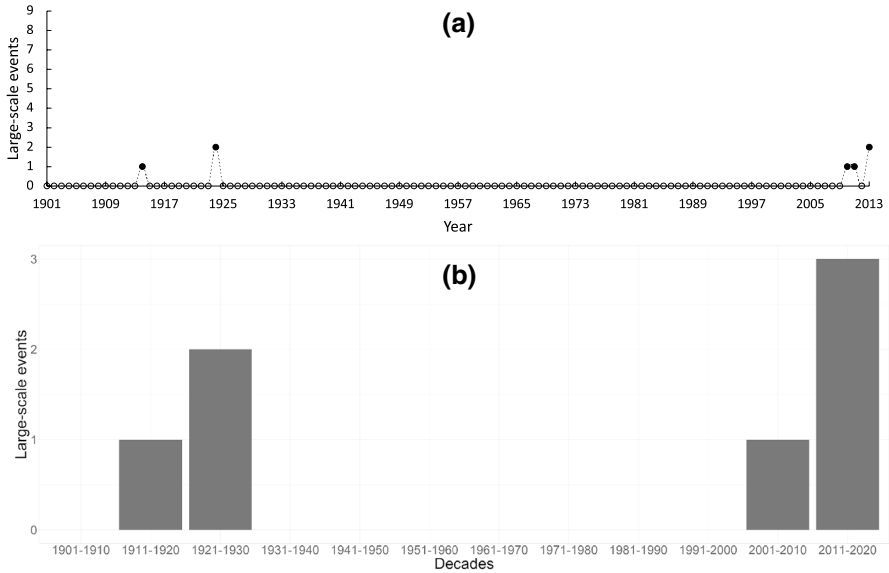
Fig. 8 a Frequency of large-scale events from 1901–2013 when rainfall depths exceed 90th percentile threshold at least 75% (or 42 out of 55 grid points) in the Upper Ganges Catchment. **b** Frequency of large-scale events at the decadal scale. The last decade, 2011–2020, shows frequency of occurrence of large-scale events only from 2011–2013

Fig. 9 a Frequency of large-scale events from 1901–2013 when rainfall depths exceed 95th percentile threshold at least 75% (or 42 out of 55 grid points) in the Upper Ganges Catchment. **b** Frequency of large-scale events at the decadal scale. The last decade, 2011–2020, shows frequency of occurrence of large-scale events only from 2011–2013

Fig. 10 **a** Frequency of large-scale events from 1901–2013 when rainfall depths exceed 99th percentile threshold at least 75% (or 42 out of 55 grid points) in the Upper Ganges Catchment. **b** Frequency of large-scale events at the decadal scale. The last decade, 2011–2020, shows frequency of occurrence of large-scale events only from 2011–2013

respectively. Accordingly, June had the lowest frequency of events for the 90th and 95th percentiles with 14 and 4 events, respectively, while July had no events for the 99th percentile. Collectively, large-scale high-intensity events in the study area tend to occur in the late monsoon season (August and September). Total rainfall events for the late monsoon season were 92, 36 and 5 events as compared to 65, 19 and 2 events for the early monsoon season (June and July) for 90th, 95th and 99th percentiles, respectively (Table 1). The occurrence of rainfall events during specific periods in the monsoon season indicates a higher probability of hazards in those periods. For example, hillslopes may become saturated with water leading to increased pore water pressure in the hillslopes during rainfall events in the early monsoon season (Bartarya and Sah 1995). Subsequent rainfall events occurring during the late monsoon season should further destabilize the slopes eventually causing landslides and debris flows.

Table 1 Frequency of large-scale events during June, July, August, and September for 90th, 95th and 99th percentile thresholds

Thresholds	June	July	August	September	Total large-scale events*
90th Percentile	14	51	52	40	157
95th Percentile	4	15	15	21	55
99th Percentile	2	0	1	4	7

*Total large-scale events represent the sum of all the large-scale events in each month from June to September for each threshold value

Fig. 11 a: Time-series of last November, last December AO from 1900–2012, and time-series of January, ▶
February, and March AO from 1901–2013. Monthly values of AO for each year are shown with gray lines
and 10-year means are shown with dark lines (e.g., for January AO time-series, 10-year means are calcu-
lated for 1901–1910, 1902–1911,1903–1912 and so on). Start year of each 10-year mean window is the
mid-point of the window, e.g., 1905 represents the data point for 10-year mean for 1901–1910, 1906 for
1902–1911, and so on **b**: Time-series of April, May, June, July, August, and September AO from 1901–
2013. Monthly values of AO for each year are shown with gray lines and 10-year means are shown with
dark lines

4.4.2 Nature of monthly AO during periods of higher frequency of large-scale rainfall events

To analyze the role of AO in influencing large-scale events, we prepared time-series of
monthly AO values from 1901 to 2013. Monthly AO ranges from January to September
of a given year and November and December from previous year (called as last Novem-
ber and last December henceforth). For example, January AO time-series consist of Jan-
uary monthly AO values from 1901–2013 and last December time-series consist of last
December monthly AO values from 1900–2012. Each monthly time-series is plotted with
10-year means, for example, 10-year means of January AO time-series ranges from mean
of 1901–1910, 1902–1911, 1903–1912, …, till 2004–2013 (Fig. 11a, b).

We found earlier that higher frequency of large-scale events exceeding the 90th and
95th percentiles were present during 1901–1930 and 2011–2013, while higher frequency
of large-scale events exceeding the 99th percentile was present during 1921–1930 and
2001–2013. First, we evaluate the AO fluctuations during 1901–1930, followed by
2001–2013.

In general, we found stronger monthly AO indices from last November to March
(Fig. 11a), in comparison with monthly AO from April to September (Fig. 11b), because
stronger AO circulations are present during the winter season compared to other months of
the year (Thompson and Wallace 1998; Xue-Dong et al. 2013). For 1901–1930, we found
higher frequency of large-scale events for the 90th and 95th percentiles and stronger AO
circulations from last November to March, exceeding ± 1 AO index, and for certain years
(within 1901–1930) exceeding ± 2 AO index. We observed higher magnitudes of negative
January AO indices from 1921–1930. Next, we found that 10-year means for last November
and January fluctuated between positive and negative AO indices till 1930; while majorly
negative AO indices were present for last December; February and March 10-year means
turned negative from early 1920s till 1930 and many years beyond 1930. For 2001–2013,
we found higher negative AO indices exceeding −2 AO index for all the months from last
December to March, while higher magnitude of positive AO index exceeding + 2 AO index
is obtained only for last December. We found that 10-year means are tending toward nega-
tive AO index toward the end of the period from 2001–2013, except for last November
AO, that were tending toward positive AO. In summary, AO has the tendency to remain
in the negative phase with larger magnitudes for majority of the months from last Novem-
ber to March during periods of higher frequency of large-scale events exceeding all the
thresholds.

Further, we explored monthly AO indices during years of the highest frequency of
large-scale events for each of the percentile (Table 2). For the 90th percentile, the highest
number of events was nine during 2010. Except for the positive index of last November
(0.30) and a smaller negative index of March (−0.45), higher magnitudes of negative AO
index were obtained for last December (−3.23), January (−2.62) and February (−4.22).
For the 95th percentile, we obtained the highest frequency of large-scale events in 1924
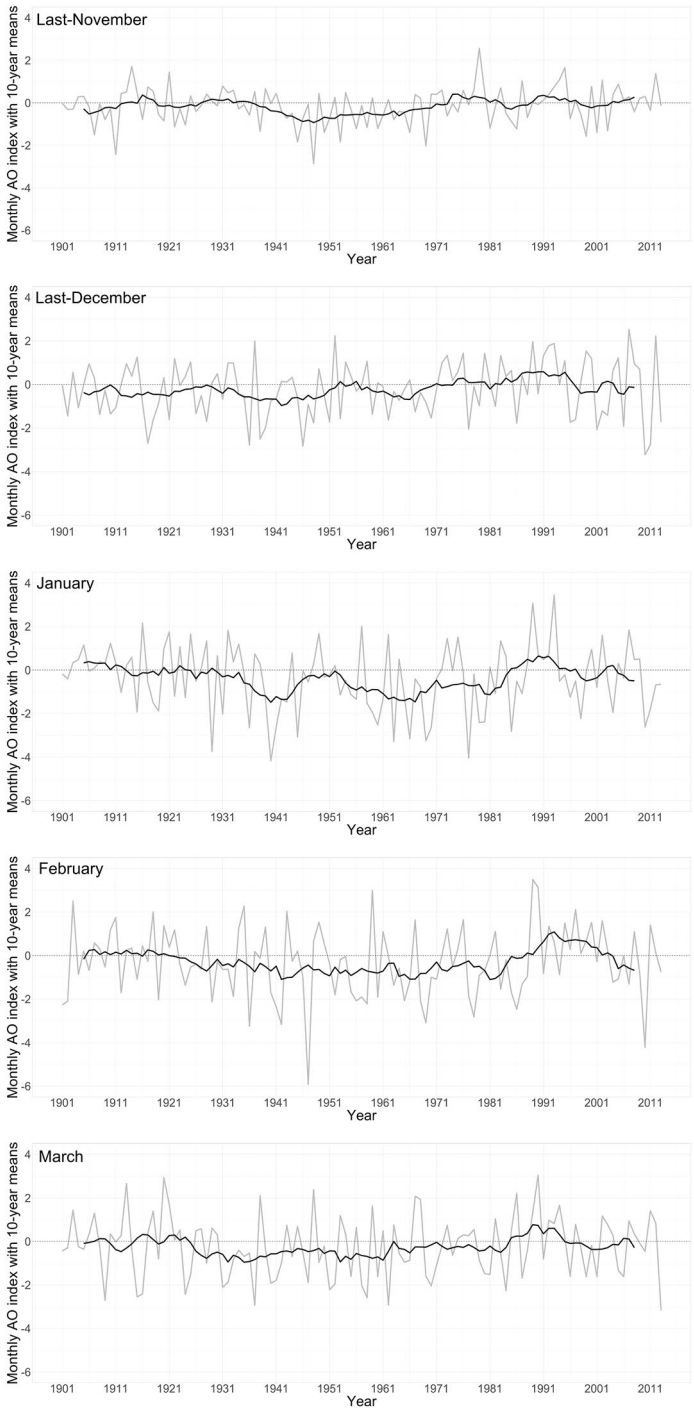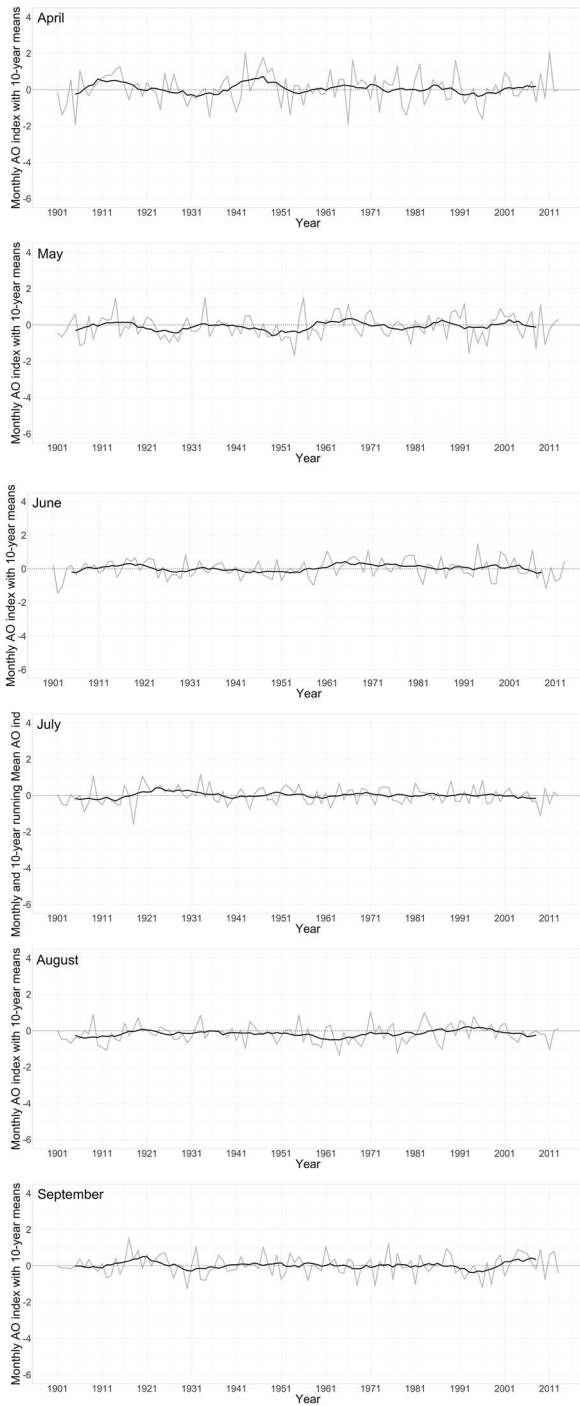
Fig. 11 (continued)

Table 2 Monthly AO indices for 90th, 95th and 99th percentile during years of the highest number of large-scale events

Thresholds	Last November	Last December	Jan	Feb	Mar	Highest rain-fall events	Years
90th	0.30	− 3.23	− 2.62	− 4.22	− 0.45	9	2010
95th	− 1.04	0.36	− 1.27	− 1.36	− 2.43	4	1924
	0.30	− 3.23	− 2.62	− 4.22	− 0.45	4	2010
99th	− 1.04	0.36	− 1.27	− 1.36	− 2.43	2	1924
	− 0.14	− 1.73	− 0.65	− 0.76	− 3.2	2	2013

and 2010 with 4 events in each year. Most of the months from last December to March had negative AO indices. For the 99th percentile, we obtained the highest frequency of large-scale events in 1924 and 2013 with two events in each year. Except for a smaller positive AO index of last December (0.36), higher magnitudes of negative AO index were obtained for rest of the months in 1924. In 2013, AO indies were negative for all the months, with a higher magnitude for March (−3.2).

4.4.3 Nature of monthly AO during periods of lower frequency of large-scale rainfall events

Lower frequency of large-scale events for all the thresholds is approximately between 1931 and 2000 (Fig. 11a, b). For the 99th percentile, we observed no large-scale event from 1931–2000. For last November and last December, we found majority of the AO phases were negative from 1931 to early 1970s and fluctuated between the two phases from early 1970s till 2000. From January to March, we found majority of the AO phases were negative from 1931 to early 1980s and fluctuated between the two phases from early 1980s till 2000. Collectively, we observed that majority of the AO phases were also negative during the lower frequency period of large-scale events.

4.4.4 Nature of monthly AO during all large-scale rainfall events from 1901–2013

We collated all the large-scale events from 1901–2013 for all the three thresholds and compared their relative occurrences under positive and negative AO scenarios from last November to March (Table 3). We found higher frequency of large-scale events, for all the

Table 3 Frequency of large-scale events for 90th, 95th, and 99th percentiles during positive (PAO) and negative AO (NAO) phase from last November to March from 1901 to 2013

Thresholds	Last November		Last December		January		February		March	
	PAO	NAO	PAO	NAO	PAO	NAO	PAO	NAO	PAO	NAO
90th Percentile	75	82	64	93	72	85	61	96	70	87
95th Percentile	27	28	24	31	24	31	17	38	23	32
99th Percentile	2	5	3	4	1	6	2	5	1	6

PAO: Positive phase of AO; NAO: Negative phase of AO

Fig. 12 Pearson correlation between monthly AO and frequency of large-scale events for depths exceed- ▶
ing **a** 90th percentile, **b** 95th percentile, and **c** 99th percentile. Years on the x-axis are the starting years of
30-year intervals. For example, 1920 represents the 30-year interval from 1920–1949. Different symbols
and colors represent monthly AO from last December to September

thresholds, during negative AO phases from last November to March, and lower frequency
during positive AO phases. For instance, for last November, 82 large-scale events exceeded
the 90th percentile during negative AO phases as compared to 75 large-scale events during
positive AO phases. Overall, large-scale events occur more frequently under negative AO
scenarios from 1901–2013 (Table 3).

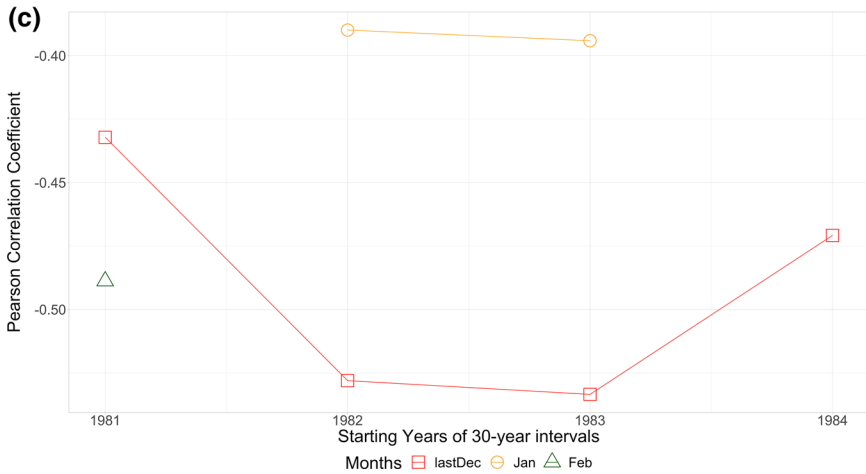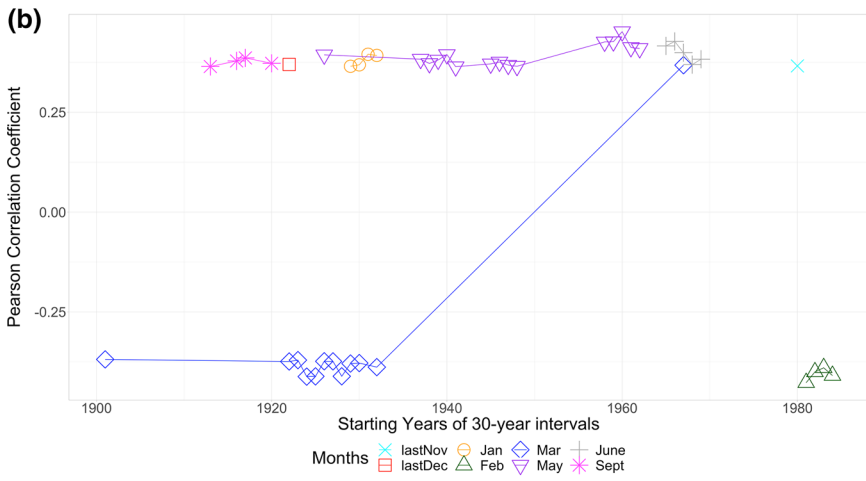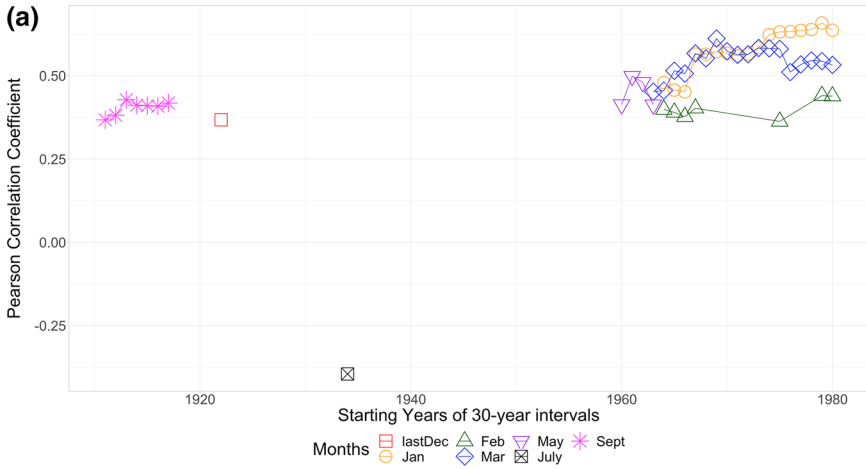### 4.4.5 Correlation between frequency of large-scale events and monthly AO from 1901–2013

We calculated Pearson correlation coefficients between frequency of large-scale events for
each percentile threshold and monthly AO values from last November to September. For
the 90th, 95th and 99th percentiles, we obtained 71, 36 and 5 years of large-scale events,
respectively, and rest of the years had zero large-scale events. For the 90th and 95th per-
centiles, we found no statistically significant correlation at 5% significance level with any
of the monthly AO time-series. For the 99th percentile, we obtained statistically significant
correlation of −0.186 with March AO at 5% significance level (p-value = 0.0482), indicat-
ing an inverse relationship, i.e., higher frequency of large-scale events for depths exceed-
ing the 99th percentile threshold is expected with more negative March AO values in the
Upper Ganges Catchment.

4.4.6 Correlation between frequency of large-scale events and monthly AO at 30-year intervals

We divided the complete time-series of large-scale events for all the percentiles into many
smaller time series of 30-year intervals ranging from 1901–1930, 1902–1931, …, till
1984–2013. We calculated correlations between monthly AO and frequency of large-scale
events for each smaller time-series of 30-year intervals.

For the 90th percentile, we found statistically significant positive correlations for peri-
ods ranging from early 1960s to late 2000s with January, February and March AO, with
higher positive correlations for January and March AO (Fig. 12a); negative correlation was
associated with the July AO from 1934–1963. For the 95th percentile, we obtained statisti-
cally significant positive correlations for periods ranging from mid-1920s to early 1990s
for the May AO; positive correlations were associated with different AO months but for
fewer number of 30-year periods (Fig. 12b). We obtained statistically significant negative
correlation for March AO from 1901–1930 and early 1920s to early 1960s. Negative cor-
relations were also associated with February AO from 1980–2013s (Fig. 12b). For the 99th
percentile, we obtained statistically significant negative correlations with last December,
January and February AO from early 1980s-early 2010s, and the lowest values of negative
correlations are associated with the last December AO (Fig. 12c).

Further, it is also important to understand the correlation behavior in the recent dec-
ades. For the period from 1950–2013, we obtained statistically significant positive cor-
relations for January, February, March and May AO for the 90th percentile; for the 95th

percentile, we obtained positive correlations for last November, March, May and June
AO, and negative correlations for February AO; and for the 99th percentile, we obtained
negative correlations for last December, January and February AO. For the period from
1901–1950, we obtained statistically significant correlation with September AO for
the 90th and 95th percentiles, and a single negative correlation with March AO from
1901–1930.

4.4.7 Correlation between frequency of large-scale events and monthly AO at 60-year intervals

We divided the complete time-series of large-scale events for all the percentiles into
many smaller time series of 60-year intervals to understand the correlation structure at
longer time periods in comparison with 30-year intervals. For the 90th percentile, we
obtained statistically significant positive correlation with January AO from early 1930s
to late 2000s, and September AO from 1913 to 1976 (Fig. 13a). For the 95th percentile,
we obtained statistically significant positive correlation with May and September AO
from early 1920s to early 1990s and 1913–1972, respectively, and statistically signifi-
cant negative correlation for February AO from early 1950s–late 1970s and April AO
from 1919–1978 (Fig. 13b). For the 99th percentile, we obtained statistically significant
negative correlations for last December AO from early 1950s-early 2010s, and February
AO from 1951–2010 (Fig. 13c).

For the period from 1950–2013, we obtained a single statistically significant posi-
tive correlation for January AO for the 90th percentile, negative correlations for Febru-
ary AO for the 95th percentile, and higher magnitudes of negative correlations for last
December and February AO for the 99th percentile.

Collectively, for the recent period from 1950–2013 and considering analysis for both
30- and 60-year intervals, we observed that AO during late winter months (January and
February) and early spring months (March to May) has positive correlations with large-
scale events associated with the 90th percentile depths. However, large-scale events
associated with the 95th percentile and extreme large-scale events associated with
the 99th percentile had negative correlations with AO during late winter months. The
inverse relationship between late winter AO months and higher frequency of large-scale
events of large magnitudes imply that more negative AO indices can cause large-scale
rainfall events of higher rainfall depths in the Upper Ganges Catchment.

4.4.8 Nature of AO during contemporary floods in the Upper Ganges Catchment

Two large floods had occurred in the Upper Ganges Catchment in 1970 and 2013. For
the 1970 flood, monthly AO indices were negative with high magnitudes during winter
and spring months, except for the positive last November AO index (last Nov: 0.41,
last Dec: − 1.54, Jan: − 2.65, Feb: − 1.0, Mar: − 2.04). For the 2013 flood, monthly
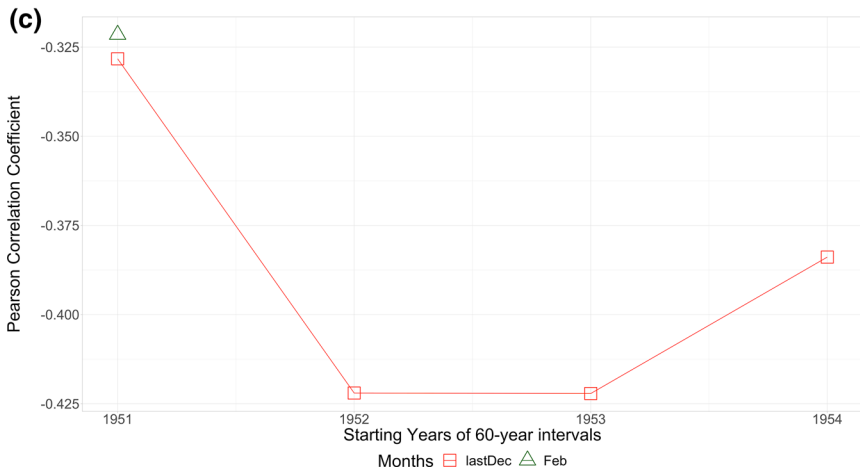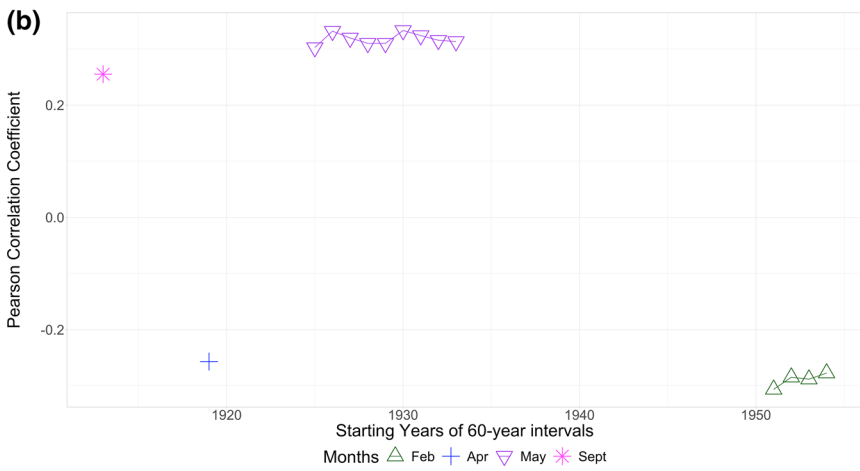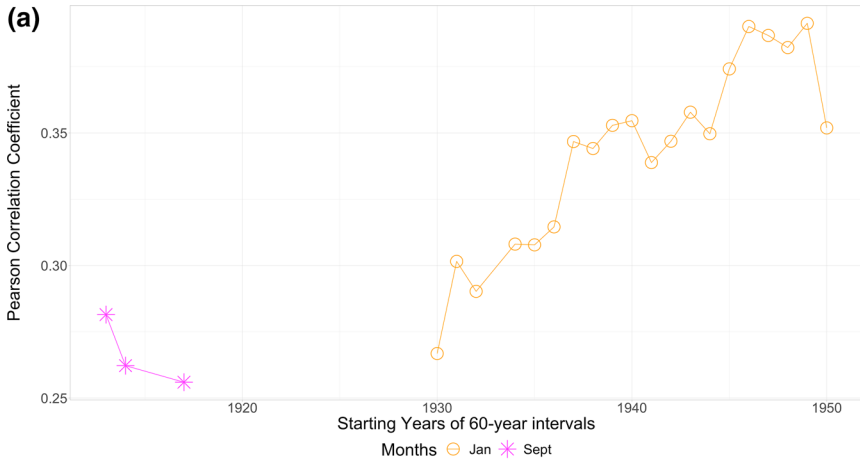
AO indices were negative with the highest value of − 3.20 during March (last Nov: − 0.14, last Dec: − 1.73, Jan: − 0.65, Feb: − 0.76, Mar: − 3.20). Collectively, we found the presence of negative AO phase during winter and spring months prior to two large floods in the Upper Ganges Catchment.

5 Conclusion

Majority of the statistically significant positive trends for both intensity and frequency of high, very high and extreme rainfall events (exceeding 90th, 95th and 99th percentile thresholds, respectively) are spatially located north as well as in the vicinity of the MCT in the Higher Himalayan region. This may lead to the occurrence of higher number of rainfall events with greater magnitudes in the Higher Himalayas where unstable and steep slopes may generate debris flows, landslides, LLOFs and flash floods during high-intensity rainfall events. The 99th percentile trends for both intensity and frequency are obtained in the vicinity of the upstream section of the Mandakini Catchment, implying that the Mandakini Catchment is at a higher risk of natural hazards in the future. This is particularly a severe situation because the 2013 flood has already increased the vulnerability of local people and tourists to a variety of natural hazards. Increasing trends for high and very high rainfall depths are located in the upstream section of Bhagirathi and Alaknanda River systems, where steep slopes, together with deep and narrow valleys, will likely increase the risk of LLOFs and flash floods in the river valleys. Trends were not found to be varying with elevations indicating that long-term trends are not dependent on the topography in the Upper Ganges Catchment. Also, higher density of trends was located in barren unculturable wasteland (or scrub lands) and evergreen forests and fewer trends were located in grasslands and snow/glacier areas.

Although it is likely that positive trends indicate a potential increase in future floods, we are careful not to claim high-intensity rainfall events as the sole drivers of flood hazard in the study area. Factors including presence of hydraulic structures, such as dams and reservoirs, snowmelt, catchment sizes, channel flow capacity and buildings on flood plains, may alter the streamflow (Do et al. 2017; Wasson and Newell 2015). For example, Do et al. (2017) indicated decreasing trends in annual maximum streamflow were occurring in tandem with increasing trends in extreme precipitation at the global scale, because of the confounding factors listed above. We recommend that streamflow records in the Higher Himalaya should be analyzed along with rainfall data to tease out the effects of the latter on the former.

Further, we explored the connection between the AO climate system and frequency of large-scale rainfall events and found negative correlations between late winter AO (last December, January and February) and frequency of large-scale rainfall events with higher rainfall depths, indicating that large magnitude of negative AO phases is more likely to influence the occurrence of extreme rainfall depths in the Upper Ganges Catchment. Also, most of the AO phases were negative during winter and spring months with high magnitudes leading up to the floods in 1970 and 2013, lending support to the notion that a negative AO phase may influence monsoon rainfall leading to floods in the Indian Himalaya. However, we have not explored the mechanisms through with AO will influence the monsoon rainfall that lead to floods. Therefore, AO is a potential climatic phenomenon that should be taken into account when analyzing hydro-climatic hazards in the Indian Himalaya.

The findings of this study can be used in climate modeling of high-intensity rainfalls and understanding their causes for the Indian region. For example, Dash et al. (2017) highlighted that 'understanding extremes' was one of the four major themes in climate modeling in India—one that was needed to strengthen the capability of climate models to simulate high-intensity events and their drivers. Further, we suggest that new research initiatives should be designed to understand the effects of climate change on the occurrence of high-intensity events in the Indian Himalaya. Arctic Amplification, which refers to the warming of the Arctic region twice as fast as the global mean, should also be studied because it influences the AO system (Cohen et al. 2014, 2020), and, therefore, may influence extreme rainfall occurrences in the Himalayas.

Compliance with ethical standards

Conflicts of interest The authors declare no competing interests.

Availability of data and material Data derived from public domain resources. The data that support the findings of this study are available at the IMD website at www.imdpune.gov.in and at the NOAA website at www.esrl.noaa.gov/psd/data/20thC_Rean/timeseries/monthly/AO/.

References

Agnihotri R, Dimri AP, Joshi HM, Verma NK, Sharma C, Singh J, Sundriyal YP (2017) Assessing operative natural and anthropogenic forcing factors from long-term climate time series of Uttarakhand (India) in the backdrop of recurring extreme rainfall events over northwest Himalaya. Geomorphology 284:31–40

Archer DR, Fowler HJ (2004) Spatial and temporal variations in precipitation in the Upper Indus Basin, global teleconnections and hydrological implications. Hydrol Earth Syst Sci Discuss, EGU 8(1):47–61

Ashok K, Guan Z, Yamagata T (2001) Impact of the Indian Ocean Dipole on the relationship between the Indian Monsoon rainfall and ENSO. Geophys Res Lett 28(23):4499–4502

Ashok K, Guan Z, Saji NH, Yamagata T (2004) Individual and combined influences of ENSO and the Indian Ocean Dipole on the Indian Summer Monsoon. J Clim 17:3141–3154

Asthana AKL, Sah MP (2007) Landslides and cloudbursts in the Mandakini Basin of Garhwal Himalaya. Himalayan Geol 28(2):59–67

Bartarya SK, Sah MP (1995) Landslide induced river bed uplift in the Tal valley of Garhwal Himalaya, India. Geomorphology 12:109–121

Behera SK, Luo JJ, Masson S, Rao SA, Sakuma H (2005) A CGCM study of the interaction between IOD and ENSO. J Clim 19:1688–1705

Bhardwaj A, Ziegler AD, Wasson RJ, Chow WTL (2017) Accuracy of rainfall estimates at high altitude in the Garhwal Himalaya (India): a comparison of secondary precipitation products and station rainfall measurements. Atmos Res 188:30–38

Bharti V, Singh C, Ettema J, Turkington TAR (2016) Spatiotemporal characteristics of extreme rainfall events over the Northwest Himalaya using satellite data. Int J Climatol 36:3949–3962

Bhutiyani MR, Kale VS, Pawar NJ (2009) Climate change and the precipitation variations in the northwestern Himalaya: 1866–2006. Int J Climatol 30:535–548

Boers N, Goswami B, Rheinwalt A, Bookhagen B, Hoskins B, Kurths J (2019) Complex networks reveal global pattern of extreme-rainfall teleconnections. Nature 566(7744):373–377

Bookhagen B (2010) Appearance of extreme monsoonal rainfall events and their impact on erosion in the Himalaya. Geomat, Nat Hazards Risk 1(1):37–50

Cohen J, Screen JA, Furtado JC, Barlow M, Whittleston D, Coumou D, Francis J, Dethloff K, Entekhabi D, Overland J, Jones J (2014) Recent Arctic amplification and extreme mid-latitude weather. Nat Geosci 7:627–637

Cohen J, Zhang X, Francis J, Jung T, Kwok R, Overland J, Ballinger TJ, Bhatt US, Chen HW, Coumou D, Feldstein S, Gu H, Handorf D, Henderson G, Ionita M, Kretschmer M, Laliberte F, Lee S, Linderholm HW, Maslowski W, Peings Y, Pfeiffer K, Rigor I, Semmler T, Stroeve J, Taylor PC, Vavrus S, Vihma T, Wang S, Wendisch M, Wu Y, Yoon J (2020) Divergent consensuses on Arctic amplification influence on midlatitude severe winter weather. Nat Clim Change 10:20–29

Coumou D, Capua GD, Vavrus S, Wang L, Wang S (2018) The influence of Arctic amplification on midlatitude summer circulation. Nat Commun 9(1):1–12

Dash SK, Mishra SK, Sahany S, Venugopal V, Karumuri A, Gupta A (2017) Climate modeling in India: present s status and way forward. Bull Am Meteorol Soc 98(8):183–188

Dimri AP, Chevuturi A (2016) Western disturbances-An Indian meteorological perspective. Springer International Publishing, Switzerland

Do HX, Westra S, Leonard M (2017) A global-scale investigation of trends in annual maximum streamflow. J Hydrol 552:28–43

Dobhal DP, Gupta AK, Mehta M, Khandelwal DD (2013) Kedarnath disaster: facts and plausible causes. Curr Sci 105(2):171–174

Ghosh S, Luniya V, Gupta A (2009) Trend analysis of Indian summer monsoon rainfall at different spatial scales. Atmos Sci Lett 10:285–290

Ghosh S, Das D, Kao SC, Ganguly AR (2012) Lack of uniform trends but increasing spatial variability in observed Indian rainfall extremes. Nat clim change 2:86–91

Goswami BN, Venugopal V, Sengupta D, Madhusoodanan MS, Xavier PK (2006) Increasing trend of extreme rain events over India in a warming environment. Science 314:1442–1445

Guhathakurta P, Sreejith OP, Menon PA (2011) Impact of climate change on extreme rainfall events and flood risk in India. J Earth Syst Sci 120(3):359–373

Hamed KH, Rao AR (1998) A modified Mann-Kendall trend test for autocorrelated data. J Hydrol 204:182–196

Hartmann H, Buchanan H (2014) Trends in extreme precipitation events in the Indus river basin and flooding in Pakistan. Atmos Ocean 52(1):77–91

Houze RA Jr, McMurdie LA, Rasmussen KL, Kumar A, Chaplin MM (2017) Multiscale aspects of the storm producing the June 2013 flooding in Uttarakhand, India. Mon Weather Rev 145:4447–4466

Ives J (2004) Himalayan perceptions. Routledge, Taylor and Francis Group, London and New York

Joseph S, Sahai AK, Sharmila S, Abhilash S, Borah N, Chattopadhyay R, Pillai PA, Rajeevan M, Kumar A (2015) North Indian heavy rainfall event during June 2013: diagnostics and extended range prediction. Clim Dyn 44:2049–2065

Joshi V, Kumar K (2006) Extreme rainfall events and associated natural hazards in Alaknanda valley, Indian Himalayan Region. J Mt Sci 3(3):228–236

Kala CP (2014) Deluge, disaster and development in Uttarakhand Himalayan region of India: challenges and lessons for disaster management. Int J Disaster Risk Reduct 8:143–152

Kar SC, Rana S (2014) Interannual variability of winter precipitation over northwest India and adjoining region: impact of global forcings. Theor Appl Climatol 116:609–623

Kendall MG (1975) Rank correlation methods. Charles Griffin, London

Krishnamurthy V, Goswami BN (2000) Indian monsoon-ENSO relationship on interdecadal timescale. J Clim 13:579–595

Krishnamurthy L, Krishnamurthy V (2014) Influence of PDO on south Asian summer monsoon and monsoon-ENSO relation. Clim Dyn 42:2397–2410

Krishnamurthy CKB, Lall U, Kwon HH (2009) Changing frequency and intensity of rainfall extremes over India from 1951 to 2003. J Clim 22:4737–4746

Krishnan R, Sugi M (2003) Pacific decadal oscillation and variability of the Indian summer monsoon rainfall. Clim Dyn 21:233–242

Kucharski F, Scaife AA, Yoo JH, Folland CK, Kinter J, Knight J, Fereday D, Fischer AM, Jin EK, Kröger J, Lau NC, Nakaegawa T, Nath MJ, Pegion P, Rozanov E, Schubert S, Sporyshev PV, Syktus J, Voldoire A, Yoon JH, Zeng N, Zhou T (2009) The CLIVAR C20C project: skill of simulating Indian monsoon rainfall on interannual to decadal timescales. Does GHG forcing play a role? Clim Dyn 33:615–627

Kulkarni A, von Storch H (1995) Monte Carlo experiments on the effect of serial correlation on the Mann-Kendall test of trend. Meteorol Z 4(2):82–85

Kumar KK, Rajagopalan B, Cane MA (1999) On the weakening relationship between the Indian Monsoon and ENSO. Science 284:2156–2159

Mann HB (1945) Non-parameteric tests against trend. Econometica 13:245–259

May W (2004) Simulation of the variability and extremes of daily rainfall during the Indian summer monsoon for present and future times in a global time-slice experiment. Clim Dyn 272:183–204

Midhuna TM, Dimri AP (2018) Impact of arctic oscillation on Indian winter monsoon. Meteorol Atmos Phys 131:1157–1167

Mishra NB, Chaudhuri G (2015) Spatio-temporal analysis of trends in seasonal vegetation productivity across Uttarakhand, Indian Himalayas, 2000–2014. Appl Geogr 56:29–41

Mukherjee S, Joshi R, Prasad RC, Vishvakarma SCR, Kumar K (2015) Summer monsoon rainfall trends in the Indian Himalayan region. Theoret Appl Climatol 121:789–802

Naidu CV, Durgalakshmi K, Krishna KM, Rao SR, Satyanarayana GC, Lakshminarayana P, Rao LM (2009) Is summer monsoon rainfall decreasing over India in the global warming era? J Geophys Res 114(D24):1–16

Nandargi S, Dhar ON (2011) Extreme rainfall events over the Himalayas between 1871 and 2007. Hydrol Sci 56(6):930–945

Pai DS, Sridhar L, Rajeevan M, Sreejith OP, Satbhai NS, Mukhopadyay B (2014) Development of a new high spatial resolution (0 . 25 ° × 0 . 25 °) Long period (1901-2010) daily gridded rainfall data set over India and its comparison with existing data sets over the region. Mausam 65(1):1–18

Pokhrel S, Chaudhari HS, Saha SK, Dhakate A, Yadav RK, Salunke K, Mahapatra S, Rao SA (2012) ENSO, IOD and Indian summer monsoon in NCEP climate forecast system. Clim Dyn 39:2143–2165

Rajeevan MN (2018) The Arctic teleconnections. Science and geopolitics of the white world. Springer International Publications, Newyork, pp 73–81

Rajeevan M, Bhate J, Jaswal AK (2008) Analysis of variability and trends of extreme rainfall events over India using 104 years of gridded daily rainfall data. Geophys Res Lett 35(L18707):1–6

Roy SS (2009) A spatial analysis of extreme hourly precipitation patterns in India. Int J Climatol 29:345–355

Roy SS (2011) The role of the north Atlantic oscillation in shaping regional-scale peak seasonal precipitation across the Indian Subcontinent. Earth Interact 15(2):1–13

Roy SS, Balling RC Jr (2004) Trends in extreme daily precipitation indices in India. Int J Clim 24:457–466

Roy SS, Goodrich GB, Balling RC Jr (2003) Influence of El Niño/souther oscillation, Pacific decadal oscillation, and local sea surface temperature anomalies on peak season monsoon precipitation in India. Clim Res 25:171–178

Salas JD, Delleur JW, Yevjevich VM, Lane WL (1980) Applied modeling of hydrologic time series. Water Resources Publications, Littleton, Colorado

Sati P, Gahalaut VK (2013) The fury of the floods in the north-west Himalayan region: the Kedarnath tragedy. Geomatics, Nat Hazards Risk 4(3):193–201

Sen PK (1968) Estimates of the regression coefficient based on Kendall's tau. J Am Stat As 63(324):1379–1389

Sharma S, Shukla AD, Bartarya SK, Marh BS, Juyal N (2017) The holocene floods and their affinity to climatic variability in the western Himalaya, India. Geomorphology 290:317–334

Sheikh MM, Manzoor N, Ashraf J, Adnan M, Collins D, Hameed S, Manton MJ, Ahmed AU, Baidya SK, Borgaonkar HP, Islam N, Jayasinghearachchi D, Kothawale DR, Premalal KHMS, Revadekar JV, Shrestha ML (2015) Trends in extreme daily rainfall and temperature indices over South Asia. Int J Climatol 35:1625–1637

Shepard D (1968) A two-dimensional interpolation function for irregularly spaced data. Proceedings of the 1968 ACM National Conference, 517–524

Shrestha AB, Bajracharya SR, Sharma AR, Duo C, Kulkarni A (2017) Observed trends and changes in daily temperature and precipitation extremes over the Koshi river basin 1975–2010. Int J Climatol 37:1066–1083

Singh RB, Mal S (2014) Trends and variability of monsoon and other rainfall seasons in Western Himalaya, India. Atmos Sci Lett 15:218–226

Srivastava P, Kumar A, Chaudhary S, Meena N, Sundriyal YP, Rawat S, Rana N, Perumal RJ, Bisht P, Sharma D, Agnihotri R, Bagri DS, Juyal N, Wasson RJ, Ziegler AD (2017) Paleofloods records in Himalaya. Geomorphology 284:17–30

Thompson DWJ, Wallace JM (1998) The Arctic Oscillation signature in the winter time geopotential height and temperature fields. Geophys Res Lett 25:1297–1300

Vellore RK, Kaplan ML, Krishnan R, Lewis JM, Sabade S, Deshpande N, Singh BB, Madhura RK, Rama Rao MVS (2016) Monsoon-extratropical circulation interactions in Himalayan extreme rainfall. Clim Dyn 46:3517–3546

Vellore RK, Bisht JS, Krishnan R, Uppara U, Capua GD, Coumou D (2019) Sub-synoptic circulation variability in the Himalayan extreme precipitation event during June 2013. Meteorol Atmos Phys 132(5):631–665

2936

Natural Hazards (2021) 105:2907–2936

Vittal H, Karmakar S, Ghosh S (2013) Diametric changes in trends and patterns of extreme rainfall over India from pre-1950 to post-1950. Geophys Res Lett 40:3253–3258

Wang H, Murtugudde R, Kumar A (2016) Evolution of Indian Ocean dipole and its forcing mechanisms in the absence of ENSO. Clim Dyn 47:2481–2500

Wasson RJ, Newell B (2015) Links between floods and other water issues in the Himalayan and Tibetan Plateau region. Pac Aff 88(3):653–675

Wasson RJ, Juyal N, Jaiswal M, McCulloch M, Sarin MM, Jain V, Srivastava P, Singhvi AK (2008) The mountain-lowland debate: deforestation and sediment transport in the upper Ganga catchment. J Environ Manage 88(1):53–61

Wasson RJ, Sundriyal YP, Chaudhary S, Jaiswal MK, Morthekai P, Sati SP, Juyal N (2013) A 1000-year history of large floods in the Upper Ganga catchment, central Himalaya, India. Quatern Sci Rev 77:156–166

Wester P, Mishra A, Mukherji A, Shrestha B (2019) The Hindu Kush Himalaya assessment Mountains, climate change, sustainability and people: Mountains, climate change Sustainability and People. Springer International Publications, NewYork

Xavier A, Manoj MG, Mohankumar K (2018) On the dynamics of an extreme rainfall event in northern India in 2013. J Earth Syst Sci 127(30):1–13

Xue-Dong C, Yong-Qi G, Dao-Yi G, Dong G, Furevik T (2013) Teleconnection between Winter Arctic Oscillation and Southeast Asian Summer Monsoon in the Pre-Industry simulation of a coupled climate model. Atmos Oceanic Sci Lett 6(5):349–354

Yadav RR (2010) Long-term hydroclimatic variability in monsoon shadow zone of western Himalaya, India. Clim Dyn 36:1453–1462

Yadav RK (2020) Changes in the large-scale circulations over north-west India, Chapter 3 in Himalayan weather and climate and their impact on the environment. Springer International Publications, NewYork

Yadav RK, Kumar KR, Rajeevan M (2009) Increasing influence of ENSO and decreasing influence of AO/NAO in the recent decades over northwest India winter precipitation. J Geophys Res 114:1–12

Yadav RK, Wang S-YS, Hu C-H, Gillies RR (2020) Swapping of the Pacific and Atlantic Niño influences on north central Indian summer monsoon. Clim Dyn 54:4005–4020

Yeo S, Kim W, Kim K (2017) Eurasian snow cover variability in relation to warming trend and Arctic Oscillation. Clim Dyn 48:499–511

Yue S, Wang CY (2004) The Mann-Kendall test modified by effective sample size to detect trend in serially correlated hydrological series. Water Resour Manage 18:201–2018

Zaz SN, Romshoo SA, Krishnamoorthy RT, Viswanadhapalli Y (2019) Analyses of temperature and precipitation in the Indian Jammu and Kashmir region for the 1980–2016 period: implications for remote influence and extreme events. Atmos Chem Phys 19:15–37

Zhan Y-J, Ren G-Y, Shrestha AB, Rajbhandari R, Ren Y-Y, Sanjay J, Xu Y, Sun X-B, You Q-L, Wang S (2017) Changes in extreme precipitation events over the Hindu Kush Himalayan region during 1961–2012. Adv Clim Change Res 8:166–175

Ziegler AD, Wasson RJ, Bhardwaj A, Sundriyal YP, Sati SP, Juyal N, Nautiyal V, Srivastava P, Gillen J, Saklani U (2014) Pilgrims, progress, and the political economy of disaster preparedness - the example of the 2013 Uttarakhand flood and Kedarnath disaster. Hydrol Process 28(24):5985–5990

Ziegler AD, Cantarero SI, Wasson RJ, Srivastava P, Spalzin S, Chow WTL, Gillen J (2016) A clear and present danger: Ladakh's increasing vulnerability to flash floods and debris flows. Hydrol Process 30:4214–4223

Publisher's Note Springer Nature remains neutral with regard to jurisdictional claims in published maps and institutional affiliations.

✎ Springer